SCIENTIFIC REPORTS

OPEN

SUBJECT AREAS:
CANCER
DRUG THERAPY

Received
17 September 2013

Accepted
25 November 2013

Published
16 December 2013

Correspondence and requests for materials should be addressed to X.-Z.Z. (xz-zhang@whu.edu.cn)

Dual-Targeting Pro-apoptotic Peptide for Programmed Cancer Cell Death via Specific Mitochondria Damage

Wei-Hai Chen, Xiao-Ding Xu, Guo-Feng Luo, Hui-Zhen Jia, Qi Lei, Si-Xue Cheng, Ren-Xi Zhuo & Xian-Zheng Zhang

Key Laboratory of Biomedical Polymers of Ministry of Education & Department of Chemistry, Wuhan University, Wuhan 430072, P. R. China.

Mitochondria are vital organelles to eukaryotic cells. Damage to mitochondria will cause irreversible cell death or apoptosis. In this report, we aim at programmed cancer cell death via specific mitochondrial damage. Herein, a functionalized pro-apoptotic peptide demonstrates a dual-targeting capability using folic acid (FA) (targeting agent I) and triphenylphosphonium (TPP) cation (targeting agent II). FA is a cancer-targeting agent, which can increase the cellular uptake of the pro-apoptotic peptide via receptor-mediated endocytosis. And the TPP cation is the mitochondrial targeting agent, which specifically delivers the pro-apoptotic peptide to its particular subcellular mitochondria after internalized by cancer cells. Then the pro-apoptotic peptide accumulates in mitochondria and causes its serious damage. This dual-targeting strategy has the potential to effectively transport the pro-apoptotic peptide to targeted cancer cell mitochondria, inducing mitochondrial dysfunction and triggering the mitochondria-dependent apoptosis to efficiently eliminate cancer cells.

Mitochondria are one type of important subcellular organelle and have been known as key factors in human metabolism, which play a critical role in apoptotic cell death[1,2]. Since the damage of mitochondria could induce the dysfunction of mitochondria and then trigger the cell death signaling cascades and the mitochondria-dependent apoptosis, mitochondria are recognized as an important therapeutic target in cancer therapy[3–6]. In the past few decades, many pathological stimuli against mitochondria or mitochondria-dependent apoptosis agents have been developed for cancer therapy[7–9]. A typical example is the amphiphilic α-helical pro-apoptotic peptide, KLA with the amino acid sequence of $(KLAKLAK)_2$, which can disrupt the mitochondrial membrane and induce mitochondria-dependent cell-free apoptosis, while remains relatively non-toxic outside of cells[10,11].

It is known that selective deliver of therapeutic agents to cancer cell mitochondria presents a significant influence on the programmed cell death in cancer therapy. However, many obstacles are generally encountered when specifically delivering the therapeutic agents to cancer cell mitochondria. To overcome these obstacles, an ideal delivery system should have good stability in the bloodstream, and specifically target cancer cells to efficiently avoid the nonspecific uptake by normal cells. In addition, the system should readily penetrate the cell membrane barrier, escape from cytoplasm, and target mitochondria to exert their pharmacological functions.

To improve the specificity of therapeutic agents for cancer cells and achieve the optimized therapeutic efficiency, active targeting strategy is a practical and attractive strategy. In this way, targeting ligands such as cytokines, monoclonal antibodies, aptamers and peptides are usually employed to specifically bind antigens and receptors overexpressed on cancer cells[12,13]. However, it can only enhance the relative cumulative amount of therapeutic agents in cells, but not accurately deliver therapeutic agents to a particular subcellular organelle of action. As we know, to enhance the therapeutic effect, many therapeutic agents need to be localized in particular subcellular organelles[14]. For example, the anticancer drug doxorubicin, which intercalates into DNA to induce cell apoptosis, should be delivered to cell nucleus to achieve effective cell growth inhibition[15,16]. Therefore, besides the active targeting function, subcellular organelle-specific target is also significantly important for improved treatment efficiency and an ideal therapeutic effect can be accomplished if combining the active and subcellular organelle-specific targeting functions together.

Here, a new dual-targeting pro-apoptotic peptide (DTP) was designed and prepared. As illustrated in Figure 1, the FA moiety (targeting agent I) of DTP has the reported ability to specifically recognize the folate receptor (FR)

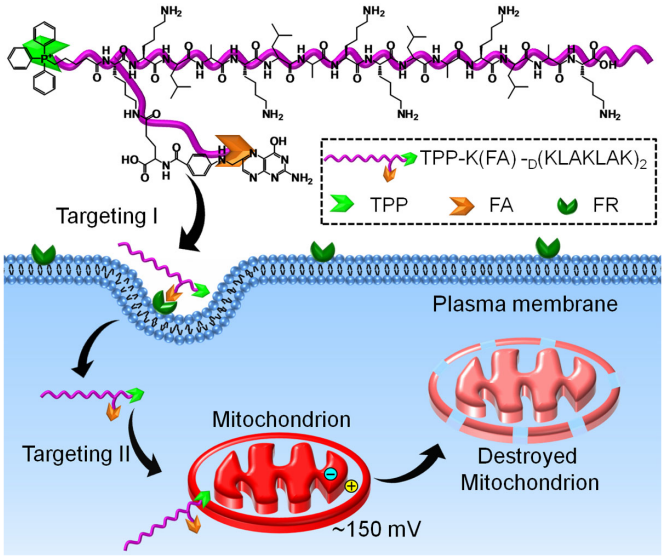

Figure 1 | Dual-targeting pro-apoptotic peptide to selectively target cancer cells and specifically damage mitochondria to lead the programmed cell death.

overexpressed on cancer cells[17], meanwhile the lipophilic and positively charged TPP moiety enables the DTP to targetly accumulate in mitochondria (targeting agent II)[18,19]. After incubation with cells, the dual-targeting property could targetedly transport DTP to the mitochondria of cancer cells. Thus, the dual-targeting strategy could effectively delivery the pro-apoptotic peptide to targeted cancer cell mitochondria, inducing the dysfunction of mitochondria and triggering the mitochondria-dependent apoptosis.

Results

Synthesis and characterization. Starting from the commercial *N*-fluorenyl-9-methoxycarbonyl (Fmoc) protected D-amino acids, the peptide (KLA) and its analogs (TPP-KLA, FA-KLA and DTP) were synthesized via Fmoc standard solid phase peptide synthesis (SPPS) technique (Supplementary Fig. S1). D-Amino acids were used to synthesize peptides for avoiding degradation by proteases in some extent[20]. It is known that the biological activity of KLA is dependent on the specific α-helical conformation[21]. Therefore, fourier transform infrared spectroscopy (FT-IR) and circular dichroism (CD) were employed to examine the secondary structure of DTP. As shown in Fig. S2 and Fig. S3, the absorbance of amide I at around 1658 cm^{-1} in the FT-IR spectra and the characteristic positive bands at around 222 nm and 208 nm in the CD spectra indicate the typical α-helical conformation adopted by DTP.

Evaluation of specific dual-targeting ability of DTP. To investigate the targeting capacity of DTP for FR ligand, cancer cell lines of KB and HeLa cells with overexpressed FR (Supplementary Fig. S4) were respectively incubated with DTP[22]. The FR-negative normal cell line of COS7 cells was also used as control. As shown in Figure 2, both DTP and FA-KLA exhibit strong inhibition of KB and HeLa cells with overexpressed FR. In contrast, due to the low level FR expression, DTP and FA-KLA do not show apparent cytotoxicity against COS7 cells. And also, because of the similar reason, KLA and TPP-KLA without of targeted folic acid moiety do not exhibit obvious cytotoxicity against either cancer cells or normal cells. Importantly to note that, the apoptotic ability of DTP against KB cells (IC_{50} = 8.2 μM) and HeLa (IC_{50} = 28.5 μM) cells is much stronger than that of FA-KLA (IC_{50} = 22 μM for KB cells and IC_{50} > 50 μM for HeLa cells). This result indicates that the cooperation of mitochondria-targeting TPP moiety with cancer cell targeting folic acid moiety can strongly improve the apoptotic ability of DTP against cancer cells. That is, due to the presence of dual-targeting function, DTP could not only specifically bind FR overexpressed cancer cells but targetly enter into mitochondria, resulting in the damage of mitochondria and ultimate apoptosis of cancer cells.

Furthermore, in order to confirm the selective cytotoxicity of DTP was caused by its specific targeting to cancer cells and subcellular targeting to mitochondria, DTP was labeled by 5-carboxyfluorescein (FAM) and then respectively incubated with cancer and normal cells. From the confocal laser scanning microscopy (CLSM) images revealed in Figure 3A and B, in comparison with weak fluorescence

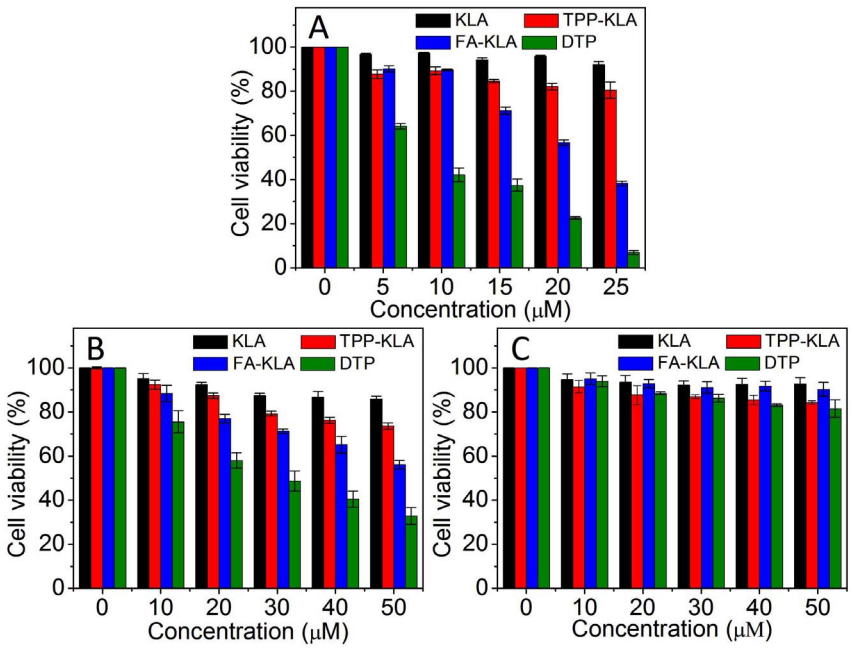

Figure 2 | Cell viability of (A) FR (++) KB cells, (B) FR (+) HeLa cells, and (C) FR (−) COS7 cells respectively incubated with KLA, TPP-KLA, FA-KLA and DTP for 48 h.

in FR-negative COS7 cells, the significant green fluorescence could be observed in FR-positive KB cells, indicating that DTP exhibited the enhanced cancerous cell internalization through the folate receptor-mediated endocytosis. More importantly, the fluorescence signals from Figure 3C and Figure 3C_{1-4} matched well and significant yellow fluorescence (overlapping regions of red and green) was found in the mitochondria, demonstrating specific mitochondria targeting ability of DTP. However, if incubating KB cells with the mixture of DTP and free folic acid (Supplementary Fig. S5), the competition between free folic acid and DTP will significantly decrease the uptake amount of DTP. The similar result is also found for the KB cells incubated with TPP-KLA. Although the presence of mitochondria-targeting function, the lack of FR-mediated endocytosis makes TPP-KLA hard to target KB cells and thus the green fluorescence is very weak (Supplementary Fig. S6). And also, although FA-KLA can target KB cells, most of FA-KLA molecules only accumulate in the cytoplasm instead of mitochondria (Supplementary Fig. S7).

The results of in vitro cytotoxicity assay and CLSM observation described above strongly demonstrate that the dual-targeting function make DTP to target cancer cells, easily escape from cytoplasm and ultimately enter into mitochondria, leading to irreversible damage of mitochondria and programmed cancer cell death.

Specific mitochondria damage of DTP. There are two well known phenotypic characteristics to evaluate the dysfunction of mitochondria, i.e., decreased mitochondrial membrane potential ($\Delta\psi$m) and decreased cellular ATP levels[23]. The loss of mitochondrial membrane potential is usually regarded as a hallmark for apoptosis since the damage of mitochondria leads to the depolarization of mitochondria with a drop in $\Delta\psi$m. In this study, mitochondrial fluorescence probe JC-1 was used to investigate the mitochondria-regulated apoptosis mechanism. From the CLSM images shown in Figure 4B and 4C, there is no obvious collapse of $\Delta\psi$m for COS7 cells incubated with DTP. The green monomer of JC-1 could enter the cytoplasm and aggregate in the normal mitochondria, with the formation of numerous red J-aggregate, which was similar to the status of COS7 cells without any treatment (Figure 4A)[24,25]. This result indicates that nearly no DTP molecules enter into the mitochondria of COS7 cells and induce the damage of mitochondria. In contrast, the disappearance of red fluorescence (normal mitochondria) and increase in green fluorescence (monomer in the cytoplasm) can be observed in KB cells incubated with DTP (Figure 4E and 4F). With the FR-mediated internalization of DTP, the mitochondria of KB cells are destroyed seriously, leading to a relatively low $\Delta\psi$m.

The relative cellular ATP level was also detected to prove the DTP-induced dysfunction of mitochondria. As displayed in Figure 5B, the relative cellular ATP of KB cells incubated with DTP significantly decreases (less than 30%) when increasing incubation period. However, the cellular ATP level of COS7 cells incubated with DTP shows no obvious change and the corresponding value is higher than 80% even after 24 h incubation (Figure 5A). As a positive control (Figure 5A and 5B), rotenone could block ATP synthesis and induce a decrease in cellular ATP level of both KB and COS7 cells. The results of mitochondrial membrane potential evaluation and relative cellular ATP level determination indicate that DTP-induced apoptosis of cancer cells is mainly built on the collapse of $\Delta\psi$m and decrease in relative cellular ATP level.

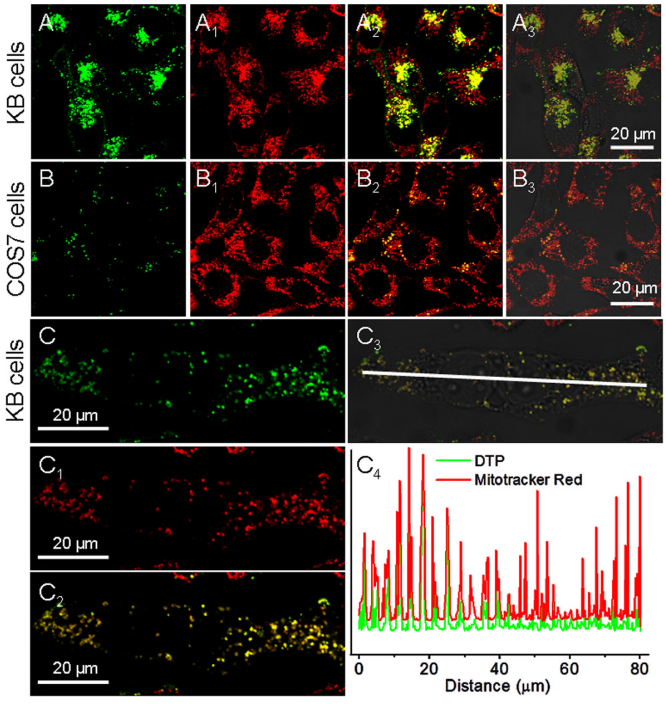

Figure 3 | CLSM images showing the dual-targeting property of DTP. (A, B, and C) Green fluorescence image. (A_1, B_1, and C_1) Red fluorescence image. (A_2, B_2, and C_2) Overlay of A and A_1, B and B_1, C and C_1, respectively. (A_3, B_3, and C_3) Overlay of A_2, B_2, C_2 and bright field images, respectively. (C_4) Fluorescence signals based on the white line in C_3. DTP was labeled by FAM (green) and mitochondria were stained with Mitotracker Red CM-H_2XRos (red). The yellow fluorescence was the overlap of DTP and mitochondria.

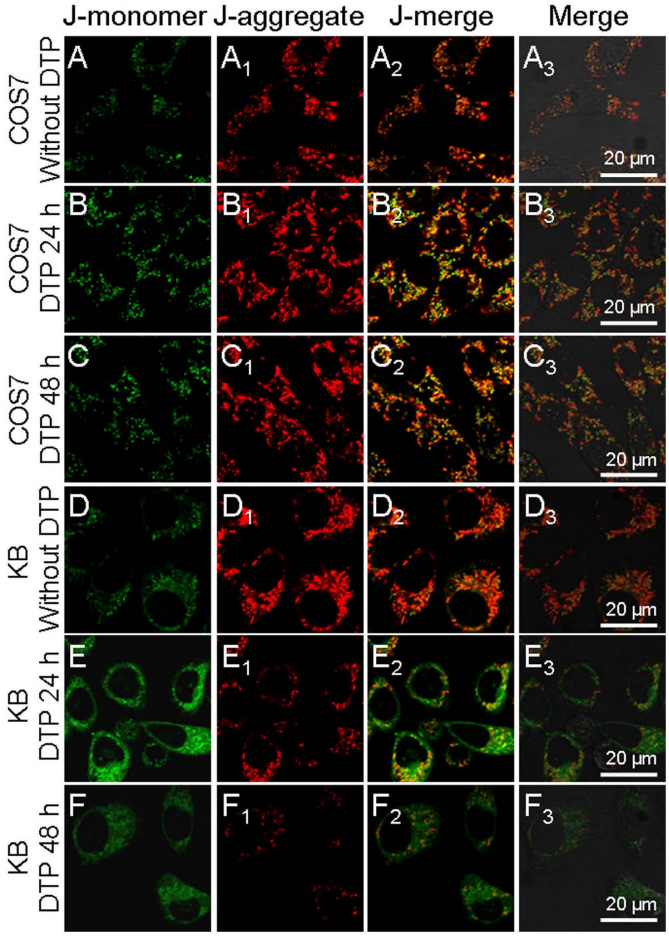

Figure 4 | Comparison of mitochondrial membrane potentials (JC-1 assay) in COS7 cells (A–C) and KB cells (D–F) by CLSM after incubation with DTP (15 μM).

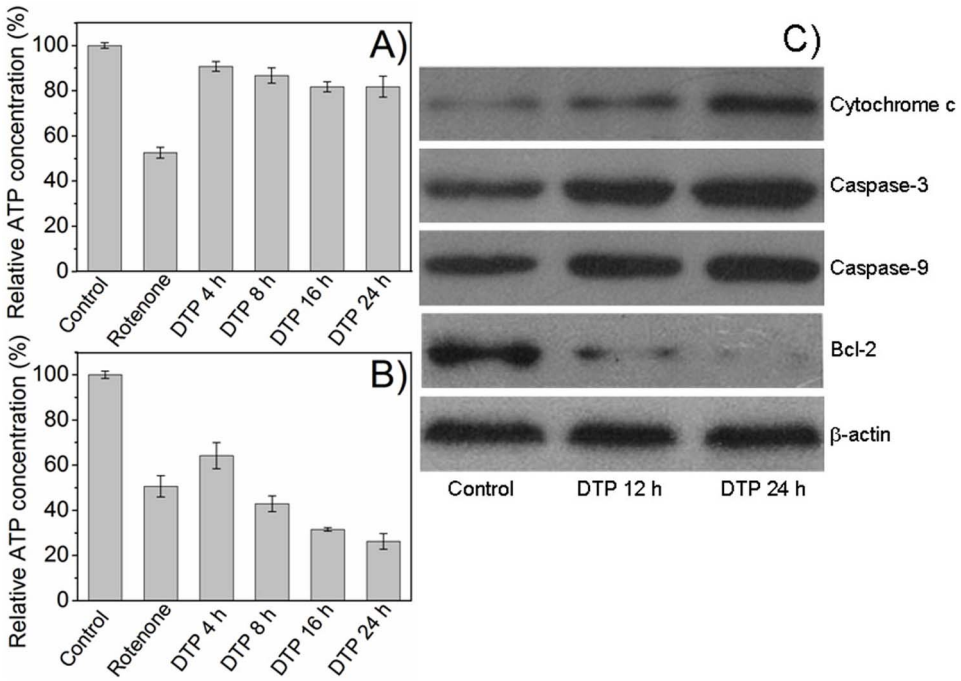

Figure 5 | Analysis of the disruption of mitochondria functions and the apoptosis of cancer cells incubated with DTP. (A) Relative ATP levels of COS7 cells after different treatments. (B) Relative ATP level of KB cells after different treatments. (C) Western blot analysis of the apoptosis-related proteins in the KB cells incubated with DTP for different time, using β-actin as the control.

Evaluation of apoptotic ability of DTP. To quantify DTP-induced mitochondria-dependent apoptosis of cancer cells, an Annexin V-FITC/PI assay was conducted. By using flow cytometry analysis, the percentage of apoptotic cells was examined after incubating KB and COS7 cells with DTP for 6 h, 12 h, 24 h and 30 h, respectively. As shown in Table 1, DTP dramatically induces the apoptosis of KB cells (around 88.8% in apoptotic rate), but does not lead to obvious apoptosis of COS7 cells (only 2.9% in apoptotic rate). The similar result can be also found in the CLSM observation. A lot of apoptotic KB cells (Annexin V-FITC positive and PI positive) can be observed with bright fluorescence (Supplementary Fig. S8). However, under the same condition, the weak fluorescence implies the rare amount of apoptotic COS7 cells (Supplementary Fig. S9). All these results are accordant with the result of in vitro cytotoxicity assay described above, indicating the superior performance of DTP to targetedly damage cancer cells without destroying normal cells.

Investigation of apoptotic mechanism. In the intrinsic mitochondrial pathway of apoptosis, a variety of events relating with mitochondria will occur, such as the release of caspase-activating proteins (cytochrome c), the depolarization of mitochondria with the loss of mitochondrial membrane potential, the disruption of electron transport, oxidative phosphorylation, the ATP production for cell metabolism, and participation the interaction with Bcl-2 family proteins[26–29]. Although we have demonstrated that the DTP-induced apoptosis of cancer cells is mainly attributed to the collapse of mitochondrial membrane potential (Figure 4E and 4F) and decrease in relative cellular ATP level (Figure 5B), the systemically apoptotic mechanism for DTP is explored here. As shown in Figure 5C and Fig. S10, the apoptosis-related proteins in KB cells are detected by western blot analysis. After incubation with DTP for 12 h or 24 h, the expression of cytochrome c, caspase-3, and caspase-9 are dramatically increased. Conversely, the expression of antiapoptotic Bcl-2 protein is significantly inhibited. Obviously, those results demonstrated that the apoptotic pathway triggered by DTP was the typical mitochondria-mediated.

Table 1 | Quantification of apoptosis and necrosis of the cells incubated with DTP (25 μM) for different time using Annexin V-FITC/PI assay

	6 h		12 h		24 h		30 h	
	KB	COS7	KB	COS7	KB	COS7	KB	COS7
Apoptosis (%)	30	3.6	54.1	2.8	62.2	3.9	88.8	2.9
Necrosis (%)	3.9	2	4.4	2.4	4.2	2.1	4	1.9

Furthermore, transmission electron microscope (TEM) was employed to directly investigate the damage of mitochondria and observe the morphology of the mitochondria before and after DTP treatment. As displayed in Figure 6A, normal morphological mitochondria (circle) and nucleus can be observed for the KB cells incubated with no DTP. However, after 12 h incubation with DTP (Figure 6B), the mitochondria in the KB cells show abnormal swelling (circle) and vacuolization (pentacle) in which the structure of cristae turns obscure. Moreover, the mitochondrial membrane is ruptured and the matrix leak out (arrow). And besides the disruption in mitochondria, the nucleus also presents a typical apoptotic characteristic, i.e., chromatin condensed into large dense masses (doji star).

In general, the damage of mitochondria will lead to the loss of mitochondrial functions and ultimate apoptosis. In the present study, DTP could induce the changes including the depolarization of mitochondria with a drop of $\Delta\psi m$, the downregulation of the antiapoptotic protein Bcl-2, and the decrease of cellular ATP level. As a cell survival mechanism, autophagy will be triggered to further provide the nutrition (ATP and amino acids) for metabolism via degrading the damaged organelles[30–32]. As presented in Figure 6C, several autophagosomes can be observed in the cytoplasm and the number of mitochondria reduced. The image with a higher magnification (Figure 6D) shows that the mitochondria (arrow) are surrounded by multiple-membranes and the autophagosomes

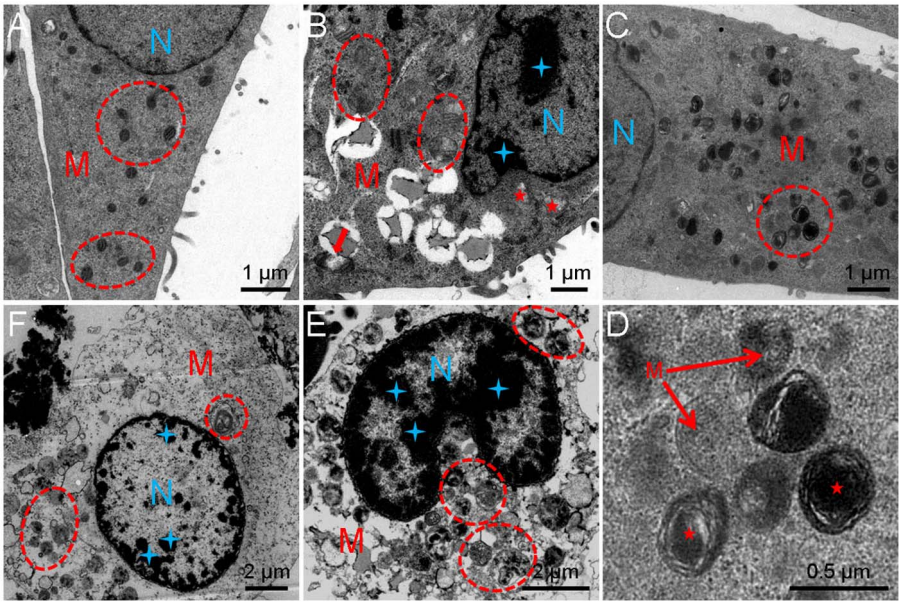

Figure 6 | TEM images of (A) KB cells incubated with no DTP, (B) and (C) KB cells incubated with DTP (20 μM) for 12 h, and (D) enlarged circled area in (C). (E) and (F) KB cells incubated with DTP (20 μM) for 24 h. Mitochondria (M) are highlighted by red circles and red pentacles. Nucleus (N) is highlighted by blue doji stars.

(pentacle) contain membranous whorls or electron-dense organelles. These morphological features represented the typical autophagic characteristics.

Also as we know, proteins of the Bcl-2 family have antiapoptotic activities and could regulate the mitochondrial pathway of apoptosis. The downregulation of Bcl-2 is also proposed to be a signal for the activation of autophagy[34,37–39]. However, the selective elimination of mitochondria or such massive degradation of essential cellular structures by autophagy would cause the irreversible cell death[33–36]. Therefore, the mitochondria are involved in the integration of apoptotic and autophagic cell death. This biological phenomenon can also found in KB cells incubated DTP. Especially in the late apoptotic stages (Figure 6E), many double-membrane bound autophagosomes contain the damaged mitochondria and swollen mitochondria with expanded cristae (circle) can be observed. The chromatin were condensed and broken in the nuclei (doji star). Even some cells (Figure 6F) are in the final apoptotic stage and show extensive vacuolization of cytoplasm, which only contained little organelles and autophagosomes (circle). Besides, the nucleus was condensed and disrupted (doji star). These morphological features are the typical apoptotic characteristics.

Discussion

The targeted delivery of a drug to cancer cells has been promised in the past decades, but does not achieve optimal effect that was hoped for[14,40]. Specific drug delivery remains a considerable challenge in cell level and many drug targets are localized in particular subcellular organelles. Subcellular targeting strategy has great potential to exert the action of drug and thereby enhances the therapeutic index, which is promising to revolutionize the way of drug design and delivery. In this report, the pro-apoptotic peptide sequence of DTP was decorated with folic acid and TPP cation, which endow the drug delivery system with dual-targeting property to hunt cancer cells selectively. After the receptor-mediated endocytosis, DTP can target cancer cells, accumulate in mitochondria and finally exert its pharmacological action. The collapses of $\Delta\psi m$, up-regulation of the caspase-activating proteins (cytochrome c) as well as the increase expression of caspase-3 and caspase-9, are the typical features of mitochondria-mediated apoptotic pathway. The dysfunction of mitochondria leads to the decrease of cellular ATP level and down-regulation of the antiapoptotic protein Bcl-2, which result in the autophagic death of cancer cells. The subcellular targeting strategy demonstrated here is expected to have promising applications in cancer therapy.

Methods

Materials. JC-1 (5,5′,6,6′-tetrachloro-1,1′,3,3′-tetraethylbenzimidazolycarbocyanine iodide) fluorescent dye, adenosine 5′-triphosphate (ATP) bioluminescent assay kit, Annexin V-FITC apoptosis detection kit and RPMI-1640 Medium were purchased from Sigma-Aldrich. Dulbecco's Modified Eagle's Medium (DMEM), fetal bovine serum (FBS), 3-[4,5-dimethylthiazol-2-yl]-2,5-diphenyltetra-zoliumbromide (MTT), trypsin, penicillin-streptomycin and Dulbecco's phosphate buffered saline (PBS) were purchased from Invitrogen.

Chemical synthesis. Details of the synthesis of pro-apoptotic peptide and its analogs are shown in Supplementary data.

Characterization. FT-IR spectra of the pro-apoptotic peptide and its analogs were collected on a Perkin-Elmer spectrophotometer by pressing the lyophilized peptide samples into KBr pellets. CD spectra were performed on a Jasco J-810 spectropolarimeter (Jasco, Japan) before respectively dissolving the pro-apoptotic peptide and its analogs in a PBS buffer (pH 7.4, 10 mM) containing 25 mM of sodium dodecylsulfate (SDS).

Cell culture. Human cervix carcinoma cells (HeLa) and African green monkey kidney fibroblast cells (COS7) were incubated in DMEM medium with 10% FBS and 1% antibiotics (penicillin-streptomycin, 10000 U/mL) at 37°C in a humidified atmosphere containing 5% CO_2. Human mouth epidermal carcinoma cells (KB) were cultured in folic acid-depleted RPMI-1640 media supplemented with 10% FBS and 1% antibiotics (penicillin-streptomycin, 10000 U/mL) at 37°C in a humidified atmosphere containing 5% CO_2.

In vitro cytotoxicity. MTT assay was used to analyze the cytotoxicity of the pro-apoptotic peptide and its analogs against KB, HeLa and COS7 cells. Briefly, KB, HeLa and COS7 cells were respectively seeded in 96-well plates at a density of 6000 cells/well, and then cells were incubated in 100 μL RPMI-1640 media (folic acid-depleted) supplemented with 10% FBS and 1% antibiotics for KB cells or DMEM containing 10% FBS and 1% antibiotics for HeLa and COS7 cells 1 day prior to adding a particular agent (KLA, TPP-KLA, FA-KLA, and DTP). After co-incubation for 2 days, the medium was replaced with 200 μL of fresh medium. Then 20 μL MTT solutions (5 mg/mL) was added to each well and further incubated for 4 h. After that, the medium was removed and 200 μL DMSO was added. The absorbance was measured at 570 nm using a microplate reader (Bio-Rad, Model 550, USA). The relative cell viability was calculated as: cell viability = $(OD_{570\ (sample)}/OD_{570\ (control)}) \times 100\%$, where $OD_{570\ (control)}$ was obtained in the absence of peptide analogs, and $OD_{570\ (sample)}$ was obtained in the presence of KLA, TPP-KLA, FA-KLA, or DTP. Each value was averaged from four independent experiments.

Confocal laser scanning microscopy. The cancer cell line of KB and normal cell line of COS7 were seeded respectively in a glass bottom dish at a density of 1×10^5 cells/well for 24 h. Thereafter, for KB cells, a particular agent (15 μM of TPP-KLA-FAM, 15 μM of FA-KLA-FAM, 15 μM of DTP-FAM, and 15 μM of DTP-FAM with (1 mM) free acid) dispersed in RPMI 1640 medium (folic acid-depleted) with 10% FBS and 1% antibiotics was added and the cells were further incubated at 37°C for another 12 h. In case of COS7 cells, a particular agent (15 μM of TPP-KLA-FAM, 15 μM of FA-KLA-FAM, 15 μM of DTP-FAM, and 15 μM of DTP-FAM with (1 mM) free acid) dispersed in DMEM containing 10% FBS and 1% antibiotics was added and the cells were also allowed to incubate at 37°C for another 12 h. To observe the specific mitochondria targeting ability of DTP, after 12 h incubation of KB cells with DTP-FAM (15 μM), the cells were further incubated with the fresh medium for 12 h. Subsequently, 100 nM Mito Tracker Red CM-H_2XRos in DMEM (without FBS to prevent the oxidization of Mito Tracker Red CM-H_2XRos) was added to stain the mitochondria for 30 min. After washing with PBS for three times, the cells were observed under a laser scanning confocal microscopy (CLSM, Nikon C1-si TE2000, BD Laser).

Study on the mitochondria-regulated apoptosis by JC-1 assay. KB and COS7 cells were respectively cultured with 15 μM DTP in cell culture dish. After 24 h or 48 h incubation at 37°C, the mitochondria were stained with JC-1 (10 μg/mL) in DMEM for another 30 min. After washing with PBS for 3 times, the cells were observed under a laser scanning confocal microscopy.

Apoptosis analysis by flow cytometry and confocal laser scanning microscopy. KB and COS7 cells were respectively seeded in 24-well plates at a density of 5×10^4 cells/well. After 24 h incubation, 25 μM DTP was added and the cells were allow to incubated for another 6 h, 12 h, 24 h, and 30 h, respectively. After washing with PBS for 3 times, the cells were digested by trypsin (no EDTA), collected in centrifuge tube, wished with PBS for 3 times and finally resuspended in 0.5 mL annexin-binding buffer. Thereafter, 5 μL Annexin V-FITC and 10 μL propidium iodide (PI) were respectively added. After 5 min incubation in dark and the subsequently washing with annexin-binding buffer twice, the cells were observed by using a laser-scanning confocal microscope and analyzed by flow cytometry (BD FACSAria TM III).

Measurement of cellular ATP levels. KB and COS7 cells were respectively seeded at a density of 2×10^5 cells per well and then incubated for 1 day prior to experiments. Cells were then treated with DTP (20 μM) for a particular time (4 h, 8 h, 16 h, and 24 h) or rotenone (1 μM) for 4 h in RPMI-1640 media (folic acid-depleted) supplemented with 10% FBS and 1% antibiotics for KB cells or DMEM containing 10% FBS and 1% antibiotics for COS7 cells at 37°C. Thereafter, the cells were washed with PBS, harvested with trypsin/EDTA for 3 min at 37°C. Complete media was added to terminate the reaction and cells were collected by centrifugation. The cells were then lysed with 70 μL 1% TCA/4 mM EDTA for 20 min on ice, followed by 35 μL Tris buffer (pH 7.4, 1 M)[41]. ATP level was assessed using the adenosine 5′-triphosphate (ATP) bioluminescent assay kit (Sigma-Aldrich) and a chemiluminometer (Lumat LB9507, EG&G Berthold).

Western blotting analysis of apoptosis-related proteins. KB cells were seeded in 24-well plates at a density of 5×10^4 cells/well and cultured with 1 mL RPMI-1640 media (folic acid-depleted) supplemented with 10% FBS and 1% antibiotics for 1 day. Then, 20 μM DTP was added and the cells were allowed to culture for 12 h and 24 h respectively. After washing with PBS for 3 times, the cells were lysed using 50 μL RIPA buffer (PBS, 1% NP-40, 0.5% Na-deoxycholate, 0.1% SDS, 10 μg/mL PMSF, 2 μg/mL aprotinin, and 100 mM Na-orthovanadate) and resuspended in 50 μL 2 × SDS sample buffer containing 1% β-mercaptoethanol. Subsequently, the samples were boiled for 5 min and separated on a 10% SDS-PAGE (15 μL per lane). After electrophoresis, the proteins were transferred to a PVDF membrane (Millipore) by semi-dry transfer cell (Bio-rad). After blocking in PBS solution (containing 5% skim milk) for 1 h, the proteins (cytochrome c, caspase-3, caspase-9 as well as Bcl-2) were detected by respectively incubating the membranes with mouse monoclonal anti-cytochrome c antibody (1 : 3000 dilution, EPI), mouse monoclonal anti-caspase-3 antibody (1 : 3000 dilution, Cell Signaling Technology), mouse monoclonal anti-caspase-9 antibody (1 : 3000 dilution, Cell Signaling Technology), and mouse monoclonal anti-Bcl-2 antibody (1 : 3000 dilution, Cell Signaling Technology) overnight at 4°C and subsequently treated with the secondary antibody HRP-labeled goat anti-rabbit IgG (1 : 3000 dilution, Santa Cruz Biotechnology) for 1 h. Specific proteins were detected by enhanced chem-iluminescence (ECL; Pierce). Mouse monoclonal anti-β-actin antibody (Santa Cruz Biotechnology) was used as protein loading control.

Observation specific damages of mitochondria by TEM. To investigate and study the specific damage of mitochondria by DTP, KB cells were respectively cultured with 20 μM DTP for 12 h and 24 h. After washing with PBS for 3 times, the cells in each well were fixed with 1 mL general fixative (containing 2.5% glutaraldehyde in 0.1 M PBS) at 4°C overnight. After washing with PBS for 3 times, the cells were further stained with 4% osmium tetroxide for 0.5 h. After rinsing with distilled water, the cells were dehydrated at room temperature in a graded ethanol series of 30%, 50%, 70%, 90% and followed by rinse of 100% ethanol (10 min × 3). After dehydration, the cells were embedded in epoxy resin and the resin was stored at 55°C for 48 h to allow resin polymerization. The embedded samples were then sliced with a thickness of 50–70 nm. Finally, the cell section was stained with 5% uranyl acetate for 15 min and 2% lead citrate for 15 min before TEM observation.

Statistics analysis. The quantitative data collected were expressed as mean ± S.D. Statistical significance was analyzed by three-sample Student's text. Statistical significance was inferred at a value of $P < 0.05$.

1. Szewczyk, A. & Wojtczak, L. Mitochondria as a pharmacological target. *Pharmacol. Rev.* **54**, 101–127 (2002).
2. Pathania, D., Millard, M. & Neamati, N. Opportunities in discovery and delivery of anticancer drugs targeting mitochondria and cancer cell metabolism. *Adv. Drug Deliv. Rev.* **61**, 1250–1275 (2009).
3. Green, D. R. & Kroemer, G. The pathophysiology of mitochondrial cell death. *Science* **305**, 626–629 (2004).
4. Wen, S., Zhu, D. & Huang, P. Targeting cancer cell mitochondria as a therapeutic approach. *Future Med. Chem.* **5**, 53–67 (2013).
5. Biasutto, L., Dong, L. F., Zoratti, M. & Neuzil, J. Mitochondrially targeted anti-cancer agents. *Mitochondrion* **10**, 670–681 (2010).
6. Chen, W. H. *et al.* A new anti-cancer strategy of damaging mitochondria by pro-apoptotic peptide functionalized gold nanoparticles. *Chem. Commun.* **49**, 6403–6405 (2013).
7. Yamada, Y., Akita, H., Kogure, K., Kamiya, H. & Harashima, H. Mitochondrial drug delivery and mitochondrial disease therapy—an approach to liposome-based delivery targeted to mitochondria. *Mitochondrion* **7**, 63–71 (2007).
8. Costantini, P., Jacotot, E., Decaudin, D. & Kroemer, G. Mitochondrion as a novel target of anticancer chemotherapy. *J. Natl. Cancer Inst.* **92**, 1042–1053 (2000).
9. Spierings, D. *et al.* Connected to death: the (unexpurgated) mitochondrial pathway of apoptosis. *Science* **310**, 66–67 (2005).
10. Ellerby, H. M. *et al.* Anti-cancer activity of targeted pro-apoptotic peptides. *Nat. Med.* **5**, 1032–1038 (1999).
11. Agemy, L. *et al.* Targeted nanoparticle enhanced proapoptotic peptide as potential therapy for glioblastoma. *Proc. Natl. Acad. Sci. U. S. A.* **108**, 17450–17455 (2011).
12. Mohanty, C., Das, M., Kanwar, J. R. & Sahoo, S. K. Receptor mediated tumor targeting: an emerging approach for cancer therapy. *Curr. Drug Deliv.* **8**, 45–58 (2011).
13. Fan, N. C., Cheng, F. Y., Ho, J. A. & Yeh, C. S. Photocontrolled targeted drug delivery: photocaged biologically active folic acid as a light-responsive tumor-targeting molecule. *Angew. Chem. Int. Ed.* **51**, 8806–8810 (2012).
14. Rajendran, L., Knölker, H. J. & Simons, K. Subcellular targeting strategies for drug design and delivery. *Nat. Rev. Drug Discov.* **9**, 29–42 (2010).
15. Xu, P., Van Kirk, E. A., Zhan, Y., Murdoch, W. J., Radosz, M. & Shen, Y. Targeted charge-reversal nanoparticles for nuclear drug delivery. *Angew. Chem. Int. Ed.* **46**, 4999–5002 (2007).
16. Pan, L., He, Q., Liu, J., Chen, Y., Ma, M., Zhang, L. & Shi, J. Nuclear-targeted drug delivery of TAT peptide-conjugated monodisperse mesoporous silica nanoparticles. *J. Am. Chem. Soc.* **134**, 5722–5725 (2012).
17. Low, P. S., Henne, W. A. & Doorneweerd, D. D. Discovery and development of folic-acid-based receptor targeting for imaging and therapy of cancer and inflammatory diseases. *Acc. Chem. Res.* **41**, 120–129 (2008).
18. Smith, R. A., Porteous, C. M., Gane, A. M. & Murphy, M. P. Delivery of bioactive molecules to mitochondria in vivo. *Proc. Natl. Acad. Sci. U. S. A.* **100**, 5407–5412 (2003).
19. Robinson, K. M. *et al.* Selective fluorescent imaging of superoxide in vivo using ethidium-based probes. *Proc. Natl. Acad. Sci. U. S. A.* **103**, 15038–15043 (2006).
20. Bessalle, R., Kapitkovsky, A., Gorea, A., Shalit, I. & Fridkin, M. All-D-magainin: chirality, antimicrobial activity and proteolytic resistance. *FEBS Lett.* **274**, 151–155 (1990).
21. Javadpour, M. M. *et al.* De novo antimicrobial peptides with low mammalian cell toxicity. *J. Med. Chem.* **39**, 3107–3113 (1996).
22. Legigan, T. *et al.* The first generation of β-galactosidase-responsive prodrugs designed for the selective treatment of solid tumors in prodrug monotherapy. *Angew. Chem. Int. Ed.* **51**, 11606–11610 (2012).
23. Wagner, B. K. *et al.* Large-scale chemical dissection of mitochondrial function. *Nat. Biotechnol.* **26**, 343–351 (2008).
24. Smiley, S. T. *et al.* Intracellular heterogeneity in mitochondrial membrane potentials revealed by a J-aggregate-forming lipophilic cation JC-1. *Proc. Natl. Acad. Sci. U. S. A.* **88**, 3671–3675 (1991).
25. Perry, S. W., Norman, J. P., Barbieri, J., Brown, E. B. & Gelbard, H. A. Mitochondrial membrane potential probes and the proton gradient: a practical usage guide. *Biotechniques* **50**, 98–115 (2011).
26. Green, D. R. & Reed, J. C. Mitochondria and apoptosis. *Science* **281**, 1309–1312 (1998).
27. Xia, T., Jiang, C., Li, L., Wu, C., Chen, Q. & Liu, S. S. A study on permeability transition pore opening and cytochrome c release from mitochondria, induced by caspase-3 in vitro. *FEBS Lett.* **510**, 62–66 (2002).
28. Lakhani, S. A. *et al.* Caspases 3 and 7: key mediators of mitochondrial events of apoptosis. *Science* **311**, 847–851 (2006).
29. Kroemer, G., Galluzzi, L. & Brenner, C. Mitochondrial membrane permeabilization in cell death. *Physiol. Rev.* **87**, 99–163 (2007).
30. Levine, B. & Yuan, J. Autophagy in cell death: an innocent convict? *J. Clin. Invest.* **115**, 2679–2688 (2005).

31. Kroemer, G. & Levine, B. Autophagic cell death: the story of a misnomer. *Nat. Rev. Mol. Cell Biol.* **9**, 1004–1010 (2008).
32. Kim, I., Rodriguez-Enriquez, S. & Lemasters, J. J. Selective degradation of mitochondria by mitophagy. *Arch. Biochem. Biophys.* **462**, 245–253 (2007).
33. Tolkovsky, A. M., Xue, L., Fletcher, G. C. & Borutaite, V. Mitochondrial disappearance from cells: a clue to the role of autophagy in programmed cell death and disease? *Biochimie* **84**, 233–240 (2002).
34. Andón, F. T. & Fadeel, B. Programmed cell death: molecular mechanisms and implications for safety assessment of nanomaterials. *Acc. Chem. Res.* **46**, 733–742 (2013).
35. Shao, Y., Gao, Z., Marks, P. A. & Jiang, X. Apoptotic and autophagic cell death induced by histone deacetylase inhibitors. *Proc. Natl. Acad. Sci. U. S. A.* **101**, 18030–18035 (2004).
36. Xue, L., Fletcher, G. C. & Tolkovsky, A. M. Autophagy is activated by apoptotic signalling in sympathetic neurons: an alternative mechanism of death execution. *Mol. Cell Neurosci.* **14**, 180–198 (1999).
37. Gozuacik, D. & Kimchi, A. Autophagy as a cell death and tumor suppressor mechanism. *Oncogene* **23**, 2891–2906 (2004).
38. Pattingre, S. *et al.* Bcl-2 antiapoptotic proteins inhibit beclin 1-dependent autophagy. *Cell* **122**, 927–939 (2005).
39. Pattingre, S. & Levine, B. Bcl-2 inhibition of autophagy: a new route to cancer? *Cancer Res.* **66**, 2885–2888 (2006).
40. Gershell, L. J. & Atkins, J. H. A brief history of novel drug discovery technologies. *Nat. Rev. Drug Discov.* **2**, 321–327 (2003).
41. Pereira, M. P. & Kelley, S. O. Maximizing the therapeutic window of an antimicrobial drug by imparting mitochondrial sequestration in human cells. *J. Am. Chem. Soc.* **133**, 3260–3263 (2011).

Acknowledgments

This work was supported by the National Natural Science Foundation of China (51125014, 51233003 and 21204068), the Ministry of Science and Technology of China (2011CB606202) and the Ministry of Education of China (20120141130003).

Author contributions

W.H.C. and X.Z.Z. conceived and designed the experiments. W.H.C., X.D.X., G.F.L., H.Z.J. and Q.L. performed the experiments. W.H.C., X.D.X., S.X.C., R.X.Z. and X.Z.Z. analyzed the data and co-wrote the paper.

Additional information

Supplementary information accompanies this paper at http://www.nature.com/scientificreports

Competing financial interests: The authors declare no competing financial interests.

How to cite this article: Chen, W.-H. *et al.* Dual-Targeting Pro-apoptotic Peptide for Programmed Cancer Cell Death via Specific Mitochondria Damage. *Sci. Rep.* **3**, 3468; DOI:10.1038/srep03468 (2013).